A Letter of Intent for a Neutrino Oscillation Experiment on the Booster Neutrino Beamline: LAr1

June 13, 2012

Contact: B. Fleming, Yale University

H. Chen, C. Thorn, D. Lissauer, V. Radeka, B. Yu, G. Mahler, S. Rescia, S. Duffin, Y. Li
Brookhaven National Laboratory, Upton, NY

L. Bartoszek
Bartoszek Engineering

E. Blucher, D. Schmitz
University of Chicago, Chicago, IL

D. Kaleko, G. Karagiorgi, B. Seligman, M. Shaevitz, B. Willis
Columbia University, Nevis Labs, Irvington, NY 10533

B. Baller, H. Greenlee, J. Raaf, R. Rameika, G. Zeller
Fermi National Accelerator Laboratory, Batavia, IL 60510

M. Messier, S. Mufson, J. Musser, J. Urheim
Indiana University, Bloomington, IN 47408

W. Huelsnitz, W. C. Louis, G. B. Mills, Z. Pavlovic, R. G. Van De Water
Los Alamos National Laboratory, Los Alamos, NM 87545

L. Bugel, J. Conrad, T. Katori, C. Ignarra, B. Jones, M. Toups
Massachusetts Institute of Technology, Boston, MA

C. Mariani
Virginia Tech, Blacksburg, VA, 24061

K. McDonald
Princeton University, Princeton, NJ

J. Assadi, M. Soderberg
Syracuse University, Syracuse, NY

M. Marshak
University of Minnesotia, Minneapolis, MN, 55455

F. Cavanna, E. Church, B. Fleming, R. Guenette, O. Palamara, K. Partyka, A. Szelc
Yale University, New Haven, CT 06520

ABSTRACT

LAr1: A Large Liquid Argon Time Projection Chamber (LArTPC) to address the anti-neutrino short baseline anomalies and provide development input for very large LArTPC detectors for long baseline oscillation physics

This Letter of Intent describes a program of physics and development employing a 1kton fiducial volume Liquid Argon TPC in the on-axis Booster Neutrino beam and off-axis NuMI beam at Fermilab. The physics program will, in conjunction with MicroBooNE, definitively address the MiniBooNE short baseline anomalies. These anomalies, along with LSND, the reactor neutrino anomaly and calibration data from Gallex and Sage, hint at beyond the standard model physic observed at short baselines. This emerging story can be addressed first at Fermilab. By deploying LAr1 (and MicroBooNE) in the on axis Booster Neutrino Beamline at Fermilab, where the MiniBooNE anomalies have been observed, these signals can be checked in the most model independent way possible. This program of physics will be complementary to other programs worldwide, also working to address these hints at short baselines.

In addition to the physics program, LAr1, following the MicroBooNE model, will have a development program serving as the engineering prototype for LArTPCs for long baseline CP Violation Searches (e.g.: LBNE).

Contents

Chapter 1

Introduction

A number of recent puzzling results from short baseline neutrino oscillation experiments have piqued interest in the community for pursuing these possible hints which together suggest some beyond the standard model physics at work. These results include the anomalies from LSND [1], MiniBooNE [2, 3], a re-analysis of predicted reactor neutrino flux [4] now suggesting a deficit of reactor neutrinos, and analysis of calibration data taken by Gallex and Sage [5]. While each of these hints taken by themselves are 2-4 sigma hints, put together, they are significant and all point toward short baseline oscillations or other new phenomena.

With the MicroBooNE experiment, Fermilab will have the first opportunity to explore these hints in neutrino mode. Beyond this, Fermilab can also probe the antineutrino anomalies using the Booster Neutrino beam, but will need a two detector experiment with a larger – 1kton fiducial volume – far detector. This detector, called "LAr1", will be located at 700m, with MicroBooNE, moved to 200 m on the Booster Neutrino beamline, to serve as the near detector. Like MicroBooNE, LAr1 will combine a physics program with a detector development program for next generation Liquid Argon Time Projection Chambers (LArTPCs) for oscillation physics.

This Letter of Intent describes the hints at short baselines, a physics program with MicroBooNE and LAr1 to search for these anomalies, and a development program with LAr1 as an engineering prototype for larger LArTPCs.

Chapter 2

Motivation

Experimental results from the last decade have revolutionized neutrino physics. Most notably, the first conclusive evidence that neutrinos oscillate and have mass was observed only about 13 years ago. While this seminal discovery has answered many questions about the neutrino, it has opened even more. Particularly interesting is the question of CP Violation in the neutrino sector. Do neutrinos and anti-neutrinos oscillate at the same rate? The answer to this question could suggest neutrinos are the key to our matter dominated universe.

Neutrinos may have other unexpected properties or unexpected partner particles. Results from the LSND and MiniBooNE short baseline, ν_e appearance experiments, combined with results from MiniBooNE anti-neutrino running show anomalies which cannot be described by oscillations between the three standard model neutrinos. In addition, a re-analysis of the reactor neutrino flux suggesting an anomaly in reactor neutrino disappearance, and results from calibration data from Gallex and Sage all point towards an emerging picture of short baseline oscillations. These signals can only be explained with beyond the standard model physics such as with the existence of sterile neutrinos and other scenarios.

There is a worldwide program developing to address these short baseline anomalies including measurements using primarily accelerator neutrinos, reactor neutrinos, neutrinos from radioactive sources, and neutrinos from DAR sources, all detected in a variety of ways. This worldwide program is well described in the recent, "Light Sterile Neutrinos: A White Paper" [6]. Fermilab has also begun to study how these

anomalies may be addressed in the Fermilab program by forming a Short Baseline Task force which will have a draft report available by the end of May [7].

The Fermilab program has the advantage of testing the signals in the same beams in which the MiniBooNE anomalies have been observed, removing some model dependencies in the experimental setup. MicroBooNE will most certainly be the first accelerator based experiment to address any of the anomalies and in this model independent way – specifically the neutrino mode anomaly. With a timely construction of LAr1, it may be the first to address the anti-neutrino anomalies, again, as it will be exposed to the BNB, in as model independent a way as possible. Fermilab will then have the answer - perhaps discovery - to this short baseline puzzle.

This Letter of Intent describes the motivation for the physics program driven by the short baseline anomalies and gives an overview of the worldwide program to address this physics. Following this is a detailed description of the sensitivity of LAr1, and the beam and detector capabilities. In addition, the conceptual design for LAr1, as an engineering prototype for larger LArTPCs is discussed.

Here a 1kton fiducial volume LArTPC is assumed with the appropriate beam rate and total delivery to be able to definitively, at the 5 σ level, address the anomalies.

2.1 Short Baseline Anomalies

The LSND anomaly

The LSND experiment used a Decay at Rest (DAR) pion beam to produce a 20-53 MeV $\overline{\nu}_\mu$ beam 30m from a Scintillator target. After 5 years of data taking, they observed 89.7± 22.4 ±6.0 $\overline{\nu}_e$ appearance events above backgrounds, corresponding to a 3.8 σ evidence of oscillations. At large Δm^2 this signal cannot be accommodated with the three Standard Model neutrinos, and like the other short baseline anomalies with $\frac{L}{E}$ ∼1, implies new physics.

MiniBooNE anomalies

The MiniBooNE $\nu_\mu \rightarrow \nu_e$ experiment has observed a 3σ signal excess in neutrino mode (128.8 ±20.4 ±38.3 electromagnetic events at E_ν below 475 meV). These events, along with backgrounds, are shown in Figure 2.1. The excess events, which can be electrons or single photons, indistinguishable in MiniBooNE's Cerenkov imaging

detector, will be addressed by the MicroBooNE experiment. MiniBooNE has also observed an excess of events in anti-neutrino mode of 57.7 $\pm 18.8 \pm 22.4$ at low and somewhat higher energies as shown in Figure 2.1. Figure 2.2 shows the $\frac{L}{E}$ dependence of these events overlaid onto the LSND events. It is this signal in anti-neutrino mode that the two detector LAr1 experiment will address.

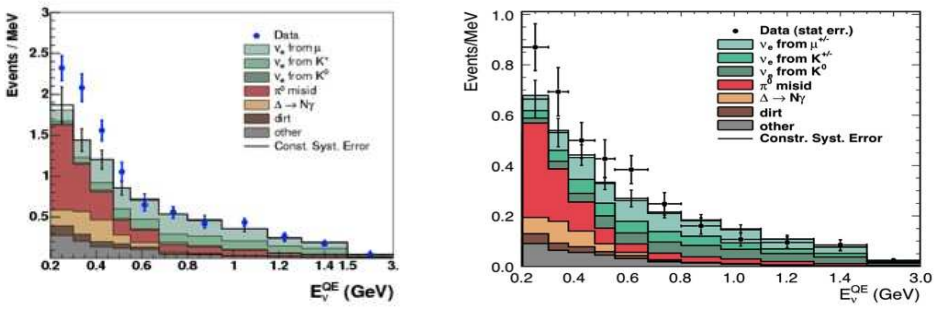

Figure 2.1: MiniBooNE anomalies. On the left, the low energy excess seen in neutrino mode, on the right, the excess seen at low and slightly higher energies in anti-neutrino mode.

Reactor Neutrino Anomaly

A new reference reactor neutrino spectra [4] prompted a re-analysis of short baseline reactor $\overline{\nu}_e$ disappearance measurements from the last several decades [8]. The re-analysis includes all the experiments listed in Figure 2.3.

The new reference spectra takes advantage of a re-evaluation of inverse beta decay cross sections impacting the neutron lifetime, and accounts for long-lived radioisotopes accumulating in reactors. Figure 2.4 shows this predicted flux compared to reactor measurements as a function of baseline of each of the experiments. With this new prediction, the reactor flux is about 6-7% higher than the average of the measurements from reactors indicating a $\overline{\nu}_e$ deficit at an $\frac{L}{E}$ consistent with the accelerator and DAR anomalies.

Gallex and Sage data

Both the Gallex and Sage solar neutrino experiments used test sources in their detectors to calibrate their detectors. In total they ran 4 test runs, 2 in Gallex and 1 in Sage with a ^{51}Cr source which emits 750 KeV ν_es, and 1 in Sage with a ^{37}Ar

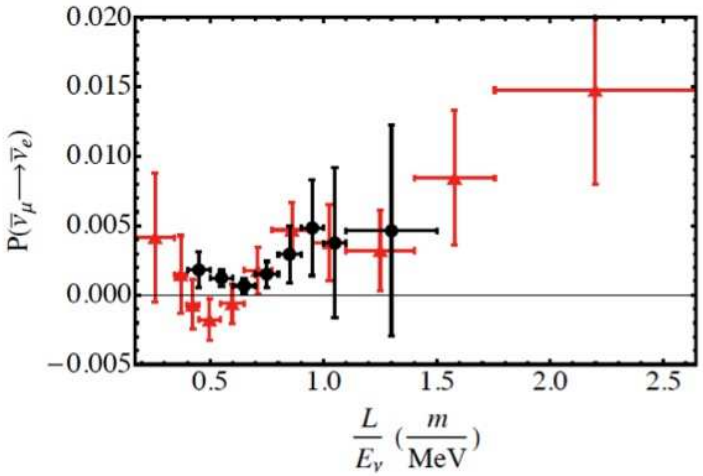

Figure 2.2: The MiniBooNE anti-neutrino events (red) overlaid on the LSND excess (black) as a function of L/E.

source, a 810 keV ν_e emitter. This test data showed a deficit of electron neutrinos as shown in Figure 2.5. The best fit Event Ratio is 0.86 ± 0.05 [5].

Interpretations

There are a number of different models that can describe all of the short baseline hints reviewed above and in detail in Reference [6]. Most of these include models with one or more sterile neutrinos and, in 3+2 models, an extra CP violating phase. As an example, Figure 2.6 shows the allowed parameter space for a 3+2 model determined from a global fit to all of the neutrino and anti-neutrino anomalies [10].

Worldwide program to address these hints

These results have generated significant interest worldwide as indicated by the number of conferences and workshops featuring this physics and by the number of proposals to address the anomalies. The different proposals to address the reactor neutrino anomalies are shown in Table 2.1. Measurements in the planning and proposal stage to look for oscillations using sources are listed in Table 2.2. Ideas to look for short baseline oscillations using DAR sources are listed in Table 2.3. The accelerator based tests are listed in table 2.4. Detailed descriptions of these many different ideas from the community exploring how to address these anomalies are described in

result	Det. type	τ_n (s)	^{235}U	^{239}Pu	^{238}U	^{241}Pu	old	new	err(%)	corr(%)	L(m)
Bugey-4	^{3}He+H_2O	888.7	0.538	0.328	0.078	0.056	0.987	0.926	3.0	3.0	15
ROVNO91	^{3}He+H_2O	888.6	0.614	0.274	0.074	0.038	0.985	0.924	3.9	3.0	18
Bugey-3-I	^{6}Li-LS	889	0.538	0.328	0.078	0.056	0.988	0.930	4.8	4.8	15
Bugey-3-II	^{6}Li-LS	889	0.538	0.328	0.078	0.056	0.994	0.936	4.9	4.8	40
Bugey-3-III	^{6}Li-LS	889	0.538	0.328	0.078	0.056	0.915	0.861	14.1	4.8	95
Goesgen-I	^{3}He+LS	897	0.620	0.274	0.074	0.042	1.018	0.949	6.5	6.0	38
Goesgen-II	^{3}He+LS	897	0.584	0.298	0.068	0.050	1.045	0.975	6.5	6.0	45
Goesgen-II	^{3}He+LS	897	0.543	0.329	0.070	0.058	0.975	0.909	7.6	6.0	65
ILL	^{3}He+LS	889	$\simeq 1$	—	—	—	0.832	0.7882	9.5	6.0	9
Krasn. I	^{3}He+PE	899	$\simeq 1$	—	—	—	1.013	0.920	5.8	4.9	33
Krasn. II	^{3}He+PE	899	$\simeq 1$	—	—	—	1.031	0.937	20.3	4.9	92
Krasn. III	^{3}He+PE	899	$\simeq 1$	—	—	—	0.989	0.931	4.9	4.9	57
SRP I	Gd-LS	887	$\simeq 1$	—	—	—	0.987	0.936	3.7	3.7	18
SRP II	Gd-LS	887	$\simeq 1$	—	—	—	1.055	1.001	3.8	3.7	24
ROVNO88-1I	^{3}He+PE	898.8	0.607	0.277	0.074	0.042	0.969	0.901	6.9	6.9	18
ROVNO88-2I	^{3}He+PE	898.8	0.603	0.276	0.076	0.045	1.001	0.932	6.9	6.9	18
ROVNO88-1S	Gd-LS	898.8	0.606	0.277	0.074	0.043	1.026	0.955	7.8	7.2	18
ROVNO88-2S	Gd-LS	898.8	0.557	0.313	0.076	0.054	1.013	0.943	7.8	7.2	25
ROVNO88-3S	Gd-LS	898.8	0.606	0.274	0.074	0.046	0.990	0.922	7.2	7.2	18

Figure 2.3: The 19 short baseline reactor experiments re-analyzed using new reactor neutrino spectra.

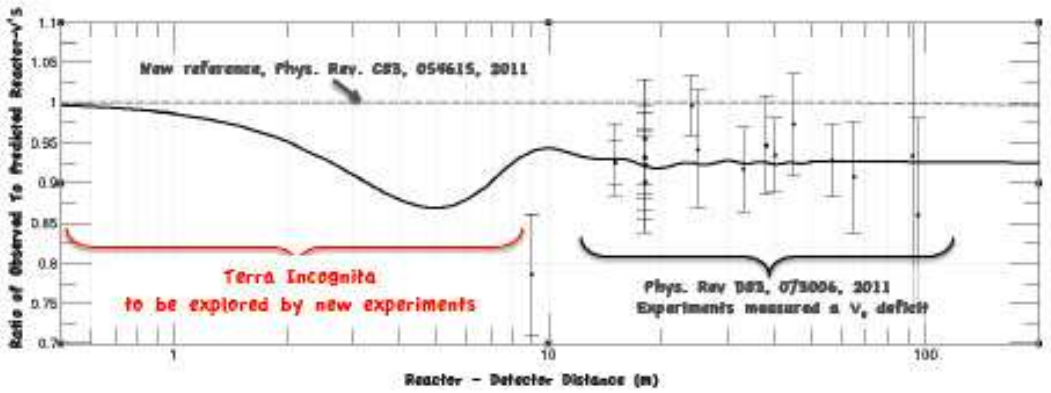

Figure 2.4: Reactor data compared to newly predicted flux as a function of baseline of each experiment. The data are on average, 6-7% below the prediction. The red and blue curves show fits to the data assuming no oscillations, and assuming oscillations in a 3+1 scenario [9].

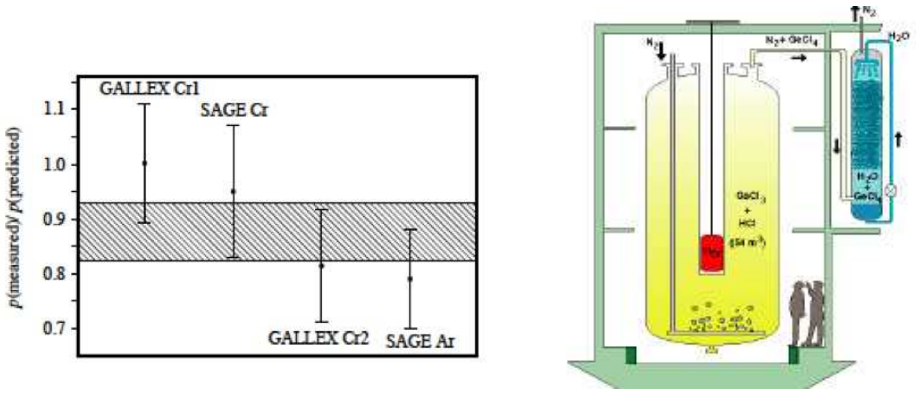

Figure 2.5: Gallex and Sage calibration data. On the right, a schematic of the source test, on the left, Gallex and Sage Measured/Predicted Event Ratio = 0.86 ± 0.05.

"Light Sterile Neutrinos: A Whitepaper".

Each of these measurements taken separately are interesting hints but without the significance necessary to drive a program of short baseline oscillations. However, understanding their collective significance, all pointing towards similar explanations such as the existence of sterile neutrinos, suggests more than just interesting hints, but rather a picture emerging of short baseline oscillation physics. Table 2.5 summarizes

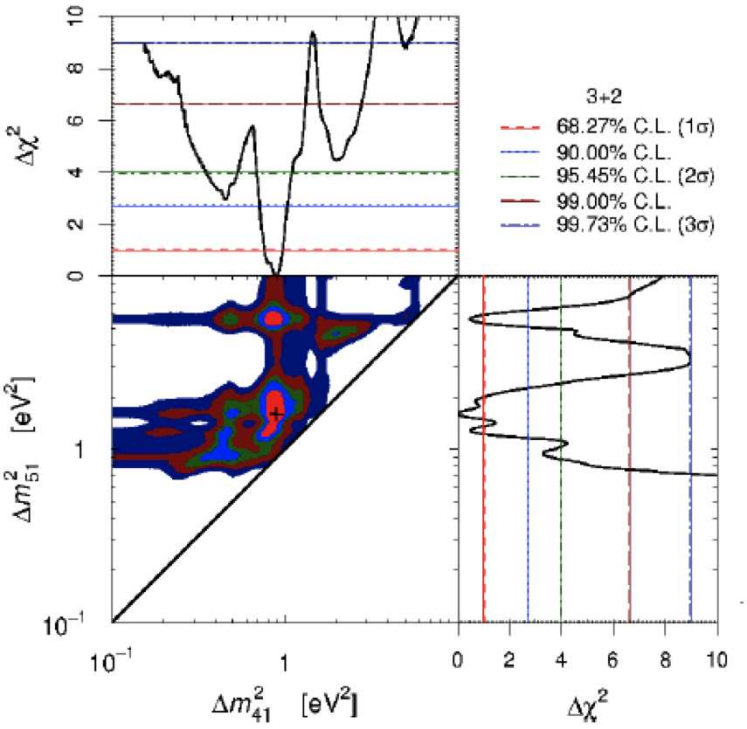

Figure 2.6: Global 3+2 fit to world neutrino and anti-neutrino short baseline data [10].

Table 2.1: Running and proposed reactor neutrino experiments to address the reactor anti-neutrino anomaly.

Experiment	Reactor	Status
Nucifer (Saclay) [11]	Osiris (70MW)	Running
DANSS (Russia) [12]	KNPP (3GW)	Fabrication
Stereo (Genoble) [13]	ILL (50MW)	Proposal
SCRAMM (CA) [14]	San-Onofre (3GW)	Proposal
SCRAMM (Idaho) [15]	ATR (150MW)	Proposal
NIST (CO) [16]	NCNR (20MW)	Proposal
NEUTRINO04 [17]	SM3 (100 MW)	Proposal

Table 2.2: Proposed Radioactive Source experiments to look for ν_e and $\overline{\nu_e}$ disappearance.

Experiment	Source and ν type	Status
Baksan [18]	$^{5}1$Cr; ν_e	Proposal
LENS [19]	$^{5}1$Cr; ν_e	Proposal
Borexino [20]	$^{5}1$Cr; ν_e	Proposal
SNO+ [20]	$^{5}1$Cr; ν_e	Proposal
Ricochet [21]	$^{3}7$Ar; ν_e	Proposal
CeLAND [22]	$^{1}44$Ce; $\overline{\nu_e}$	Proposal
Borexino [20]	$^{1}44$Ce; $\overline{\nu_e}$	Proposal
Daya-Bay [23]	$^{1}44$Ce; $\overline{\nu_e}$	Proposal

Table 2.3: Proposed experiments to look for appearance and disappearance from DAR sources.

Experiment	Source	Status
OscSNS [24]	SNS	Proposal
IsoDAR [25]	Cyclotron	Proposal

all these results and each of their significance. These hints must be explored further, both by repeating the existing measurements in an effective way, and by testing these results in a way that tests oscillation hypotheses.

Table 2.4: Running and Proposed Accelerator Experiments to look ν_e appearance, NC disappearance, and ν_μ disappearance.

Experiment	Beamline; Baseline(s); Channels	Status
MicroBooNE [26]	BNB&NuMI; 470M; ν CC, NC	Fabrication
MINOS+ [27]	NuMI ME; 750km; ν NC	Approved
LAr1 + MicroBooNE	BNB&NuMI ; 470m, 700m; $\overline{\nu}$ NC	Proposal
CERN SPS [28]	SPS ; 150m, 850mm; ν	Proposal

Table 2.5: Summary of the hints contributing to GLOBAL fits to 3+N models.

Anomaly	Type	Channel	Significance
LSND	DAR	$\overline{\nu}$ CC	3.8 σ
MiniBooNE	SBL accelerator	ν CC	3.0 σ
MiniBooNE	SBL accelerator	$\overline{\nu}$ CC	1.7σ
Gallium/Sage	Source - e capture	ν CC	2.7σ
Reactor	Beta-decay	$\overline{\nu}$	3.0σ

2.2 LAr1 sensitivity to anti-neutrino anomalies

A program to probe the MiniBooNE/LSND anomalies will be to first address the neutrino anomalies with MicroBooNE and then to re-purpose MicroBooNE as a near detector for the LAr1 detector proposed here. A near/far configuration will considerably reduce the systematic errors, while the size of the second detector will increase statistics significantly over MicroBooNE alone. The configuration proposed here is a near/far configuration at 200m/700m. The MicroBooNE detector can be moved to serve as the near detector at 200m and LAr1 can be constructed at 700m.

In the sensitivity studies presented here, the fiducial volumes assumed for MicroBooNE and LAr1 are 61.4t and 1000t respectively. The 1000t fiducial volume for LAr1 assumes a 1-2kton active volume detector. The combination of LAr1's size, beam rate, and run time are be optimized to ensure a definitive measurement. A flat 80% $\nu_e$efficiency is assumed. All results shown are for statistical errors + 5% uncorrelated systematic errors.

Figure 2.7 shows sensitivity curves to a 3+1 neutrino model, for MicroBooNE at 200m and LAr1 at 700m with a beam delivery of 10 $\times 10^{20}$ POT.

In addition to MicroBooNE and MicroBooNE +LAr1, the MINOS+ experiment, approved to begin running in 2014 when the NoVA run begins, is sensitive to sterile neutrinos through Neutral Current Disappearance. MINOS+ sensitivity is shown on the left in Figure 2.8. The green curve is the 90% confidence level limit. Combining the two experiments allows Fermilab to definitively cover and cross check these anomalies in a number of ways both at high and low Δm^2s. On the right in Figure 2.8 the MINOS+ plot is overlaid on top of sensitivities from LAr1. Note that the MINOS curve is 90% confidence level while on the LAr1 plot, the 1, 3, and 5 σ sensitivities are shown.

While the single detector MicroBooNE experiment will address the low energy excess in neutrino mode, combining two LAr detectors is clearly a very powerful way to probe short-baseline oscillations in general. This two LAr-detector experiment will offer definitive measurements of the MiniBooNE/LSND anomalies in anti-neutrino modes and therefore address the Short baseline anti-neutrino anomalies. MicroBooNE will have addressed the low-energy excess observed by MiniBooNE in neutrino mode. Further running of MicroBooNE + LAr1 in neutrino mode can probe higher energy oscillations than MicroBooNE alone. These results are shown in Figure 2.9.

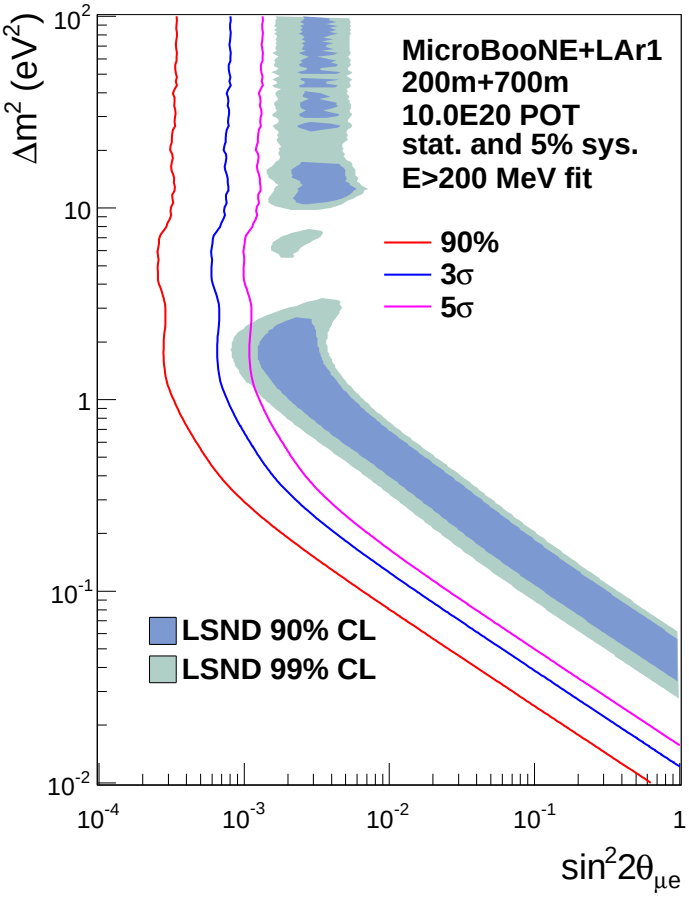

Figure 2.7: Sensitivity curves for a combined configuration with the MicroBooNE detector (as the near detector) at 200m and the LAr1 one (as the far detector) at 700m to a 3+1 neutrino model in the $\Delta m^2/sin^2 2\theta$ parameter space in anti-neutrino mode. Beam exposure is 10 $\times 10^{20}$ POT.

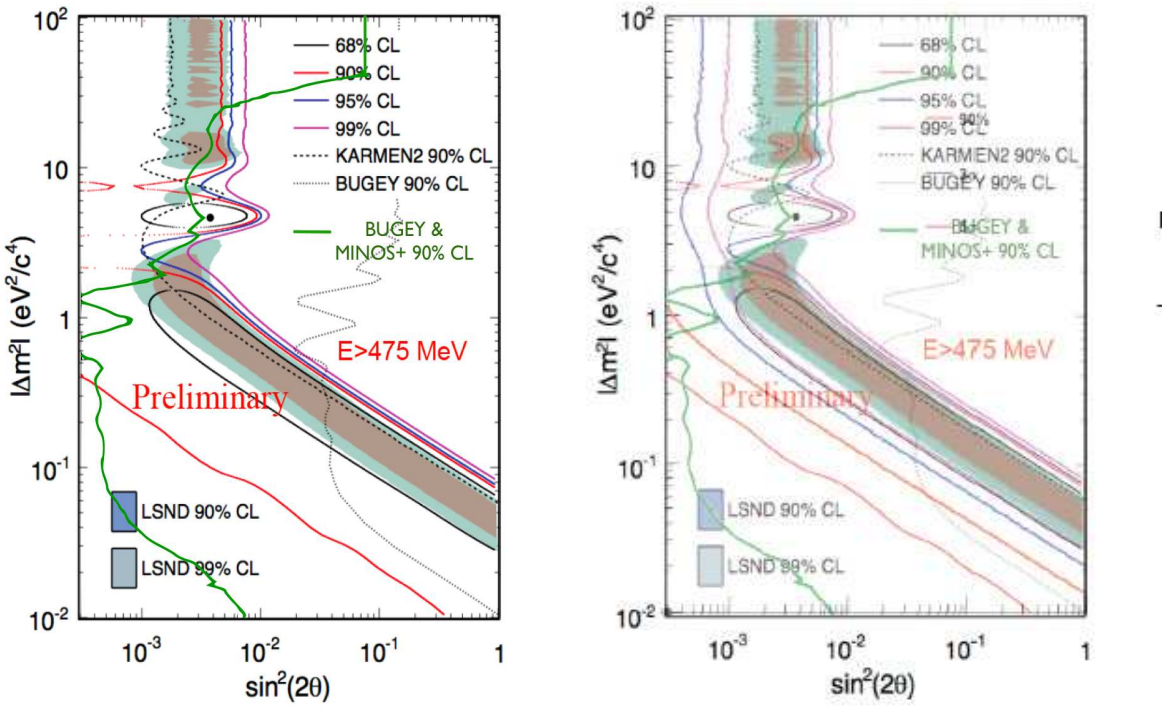

Figure 2.8: Combining sensitivities from LAr1 and MINOS+ where LAr1 is most sensitive at high Δm^2 and MINOS+ is most sensitive at low Δm^2 makes Fermilab's combined sensitivity to the LSND signal very powerful. On the left is shown MINOS+'s sensitivity to sterile neutrinos through a NC disappearance search. On the right it is overlaid on top of LAr1's sensitivity.

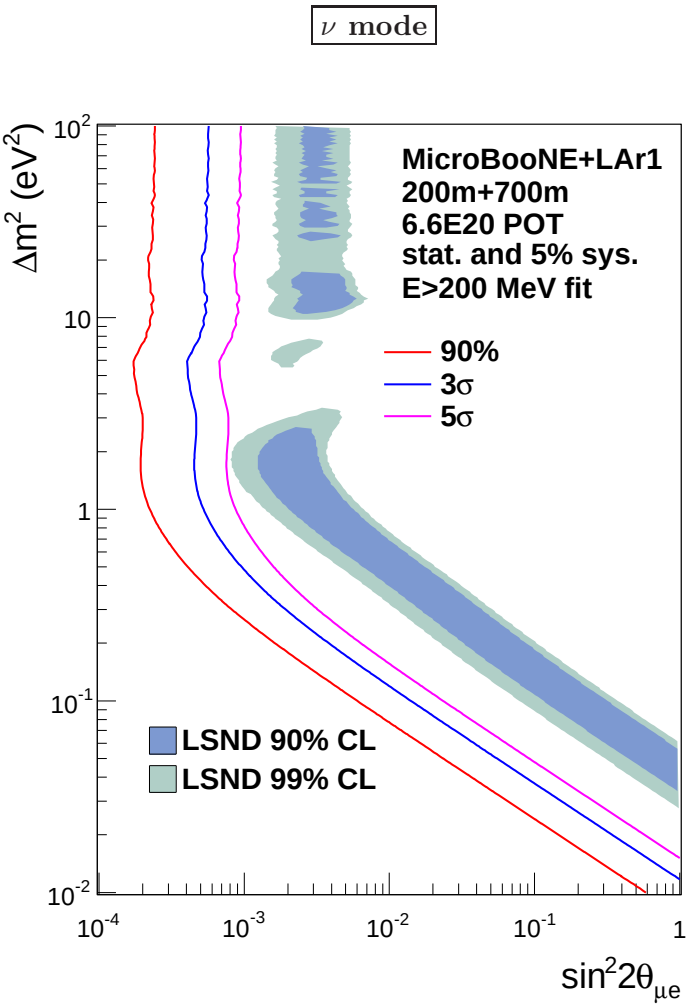

Figure 2.9: Sensitivity curves for a combined configuration with the MicroBooNE detector (as the near detector) and the LAr1 one (as the far detector) to a 2-neutrino model in the $\Delta m^2/sin^2 2\theta$ parameter space in neutrino mode with a delivery of 6.6×10^{20} POT.

Chapter 3

Detector Concept

The design of the LAr1 detector relies heavily on and is the evolution of many years of generic detector R&D and work done on MicroBooNE and LBNE [29]. The design provides a safe and cost effective way to build a large cryostat and cryogenics systems, feedthroughs, purification system, TPC, and readout and trigger systems. In addition, LAr1 can also serve as a test bed to evaluate new concepts and better designs for the yet larger LArTPCs that will enable future experiments.

The present design of LAr1 is based on a TPC constructed of an array of modular units: Anode Plane Assemblies (APAs) which contain the charge sense wires and scintillation light detection system and are instrumented with cold electronics, Cathode Plane Assemblies (CPAs) which provide the high voltage electrode to create the drift field, and Field Cage Panels which shape the uniform electric field of 500 V/cm between the APAs and CPAs. All of these active detector elements are arrayed inside a membrane style cryostat and immersed in ultra-high purity LAr maintained by the cryogenic system. The risk of a liquid argon spill is mitigated by placing all electrical and mechanical connections to the detector via feedthroughs at the top of the cryostat.

Advanced conceptual designs exist for many of the detector components such as the cold electronics and the charge collection design of the APAs. The conceptual design of the light detection system is less developed. Some systems are at a preliminary design stage and need prototyping and testing to select the best options. Beyond the LArTPC, the configuration of detector auxiliary systems is still to be

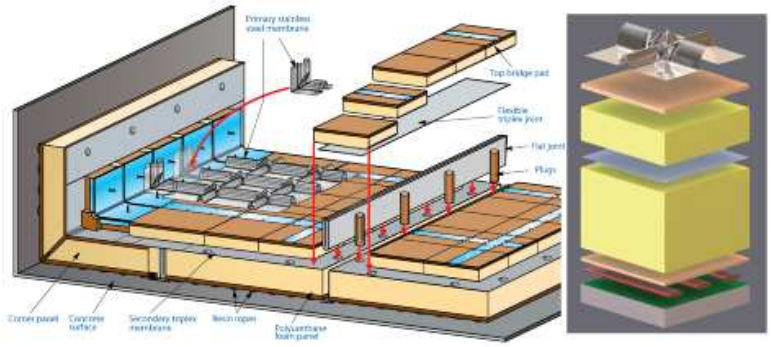

Figure 3.1: Cross Sectional view of the layers that comprise the Membrane Cryostat. Courtesy of Gaz Transport & Technigaz.

determined. For example, a downstream magnetized range-stack could be added to determine the sign and momentum of outgoing muons. Detector infrastructure, such as the cryogenic, purification, and calibration systems require further development. In short, there are many ways in which new groups would be involved in the detector modeling, hardware design and fabrication, event reconstruction, and physics analysis. In the following section we outline a conceptual design of this 1kton fiducial volume Liquid Argon detector.

3.1 Membrane Cryostat

The conceptual design for the LAr1 Detector cryostat is a rectangular vessel constructed with an industrial membrane cryostat technology extensively used for shipping Liquid Natural Gas (LNG) and for storage of LNG above ground and in caverns. Depending on the vendor, a membrane tank uses a 1.2mm - 2mm thick, stainless-steel primary liner to contain the liquid cryogen. The membrane cryostat relies on external support from a surrounding cavern or a reinforced concrete structure to support the hydrostatic load of the contents. The commercially engineered membrane system consists of the following sequence of layers, from innermost to outermost: the stainless-steel primary membrane, ∼30cm of polyurethane insulation, a thin fibgerglass-aluminum secondary membrane that contains the LAr in case of any leaks in the primary membrane; ∼50cm more insulation; a barrier to prevent water-vapor ingress and the concrete support structure (See Figure 3.1).

This in-ground tank arrangement (ie. offering access only from the top) makes optimum use of the excavated pit in which it is installed and minimizes safety concerns. The roof of the cryostat is constructed of truss-reinforced steel plate covered on the cryostat side with the insulated membrane system. All cryostat penetrations will be made through the roof. Relay racks containing the DAQ components will be located directly above each cryostat signal feedthrough.

The membrane cryostat is a robust design with a proven record spanning more than 1600 tank-years of service, predictable cost, and known installation time. There are at present two suppliers of this technology: Gaz Transport and Technigaz (GTT, France) and Ishikawajima-Harima Heavy Industries (IHI, Japan).

LAr TPCs that have operated to date have achieved good argon purity after vacuum pumping the cryostat prior to filling with LAr. Vacuum pumping is an effective means of removing oxygen and water from materials within the cryostat but purging with dry argon gas has been found to be equally effective. The purging approach has been verified in the Liquid Argon Purity Demonstrator (LAPD [30]) and is the procedure that will be used for the initial fill of MicroBooNE.

3.2 Cryogenic System

The choice of the cryogenic systems layout and location is intended to optimize safety and efficiency. It will:

- Minimize the risk of personnel injury to any Oxygen Deficiency Hazard (ODH)
- Minimize heat ingress to the cryogenic system (by minimizing piping length and pump power)
- Minimize the volume of the argon system external to the cryostat and hence minimize the potential for argon escape or contamination
- Provide safe access to refrigeration equipment that requires periodic maintenance

The re-condensers and purifiers will be located in a surface building immediately adjacent to the cryostat pit. The surface facility will include a LAr receiving dewar,

liquid nitrogen (LN) refrigerator and or a LN dewar to buffer the cooling capacity. The cryostat will hold an inventory of ∼1.3 kton of liquid argon. The required flow rate of liquid argon to be sent for purification is expected to decrease over time. The initial maximum flow rate will be 7 m^3/hr (30 gpm) . The liquid argon volume will turn over every five days at this initial maximum rate, similar to the turnover rate of the ICARUS T600 [31] detector. The purification plant will consist of duty and standby molecular-sieve columns to remove water and an activated copper columns to remove oxygen.

3.3 Time Projection Chamber and Electronics

The Time Projection Chamber (TPC) subsystem consists of three mechanical components defining the electric drift field - anode plane assemblies (APAs), cathode plane assemblies (CPAs), and field cage panels - and all the in-vessel electronics, signal and power cables, their feedthroughs, as well as the low-and high-voltage power supplies for the electronics.

3.3.1 Overview

The TPC is located inside the cryostat vessel, completely submerged in liquid argon at 89K. The TPC interfaces to the cryostat roof through TPC mounting fixtures, and it interfaces with the DAQ subsystem through the signal feedthroughs and power supplies. The TPC (Figure 3.2) consists of two rows of anode plane assemblies (APAs) between three rows of cathode plane assemblies (CPAs). Both the cathode and anode plane assemblies are 2.5m wide and 7m high. In each row, 5 such assemblies are placed edge-to-edge along the beam direction, forming an active readout area (the APA area) of 7m high by 12.7m along the beam direction. The electron drift length is 2.5m.

Each facing pair of cathode and anode rows are surrounded by a field cage, assembled from rigid G10 printed circuit sheets with parallel copper strips to create a uniform drift field.

On each anode-plane assembly, four planes of wires cover each side of a frame (the "wire frame") as shown in Figures **??**. The inner three planes of wires are oriented, going from the inside out: vertically, and at $\pm 45^o$ to the vertical, respectively. Each

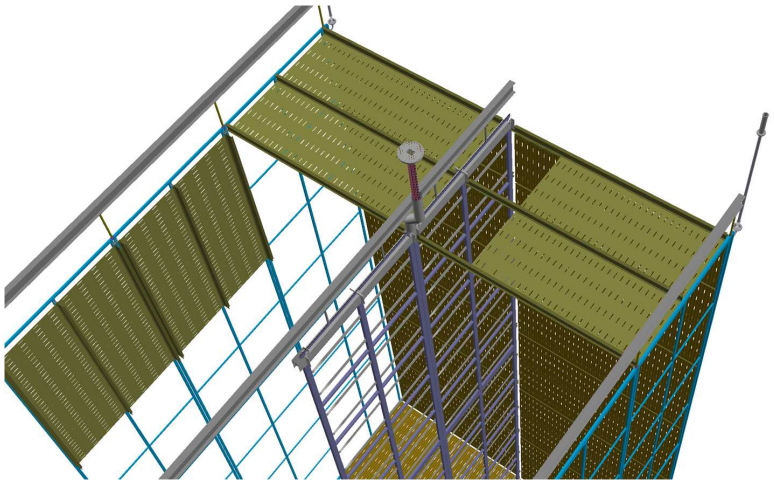

Figure 3.2: The arrangement of APAs, CPAs, and field cage panels to form the active volume of the TPC inside the cryostat. This concept illustrates one row of APAs and two rows of CPAs, where here, LAr1 will have two rows of APAs, and three rows of CPAs, however the concept remains the same.

wire is connected to a front-end readout channel. The outermost plane of wires is not connected to the readout electronics; these wires are oriented vertically. At a nominal wire pitch (center-to-center separation) of 4.5mm, the total number of readout channels is 25,600 in the entire detector.

The electronic readout chain is implemented as a CMOS ASIC designed for operation in LAr. The front-end ASIC chip utilizes a mixed-signal design. It has 16 channels of preamp, shaper and ADC followed by a large, shared buffer and the digital IO interface. Eight such chips are mounted on a single readout board, instrumenting 128 wires. A digital ASIC with an 8:1 multiplexer on this board further increases the multiplexing factor to 128:1, resulting in a single output channel for each of the 20 readout boards mounted on a single APA. Data from each of these output channels will be transmitted by a LVDS (low-voltage differential signaling) output cable through a feedthrough at the top of the cryostat.

We plan for only one cable bundle per APA, consisting of wires for low-voltage power, wire bias voltages, data out, clock in, digital control IO, and an analog monitoring output, to connect to the outside of the cryostat. Three such cable bundles will be connected through 5 feedthroughs distributed on the roof of the cryostat.

Additional feedthroughs will be required for redundant high-voltage connections (for the cathodes).

3.3.2 Requirements

The main requirements of the TPC are the following:

- Provide the means of detecting charged particles in the detector and of transmitting detector signals to the Data Acquisition System.
- Meet the physics requirement for electron/photon discrimination; we have selected the TPC wire spacing to be < 5 mm.
- Limit variation in the wire sag to < 0.5mm.
- Provide redundancy in the discrimination of electrons from photon conversions and ensure long-term reliability over the life of the experiment; we have selected a configuration of three instrumented wire planes.
- Optimize the measurement of high-energy and low-energy tracks from accelerator neutrino interactions by selecting the relative wire plane orientation.
- Enable the detector to distinguish a Minimum Ionizing Particle (MIP) from noise with a signal-to-noise ratio < 8:1.
- Enable the detector to measure the ionization up to 10 times of a MIP particle. This requirement is necessary to perform particle identification of stopping kaons and protons.
- Introduce no noise into the electronics from auxiliary detector systems.
- Enable the in-vessel electronics to operate for the life of the experiment.
- Record the wire-signal waveforms continuously without dead time.
- Use only materials that are compatible with high-purity liquid argon

3.3.3 TPC Chamber

Anode Plane Assemblies (APAs)

The anode plane assemblies (APAs) are 2.5m wide, 7m high and ∼10cm thick. Each APA is constructed from a framework of light-weight stainless-steel tubes, with four layers of wires wrapped over both sides of the frame. The front-end electronics boards are mounted on one end of the wire frame. Both stainless-steel and copper-beryllium (CuBe) wires are potential candidates. Stainless steel is the choice of ICARUS, while a copper-plated (to reduce resistance) stainless-steel wire was chosen by MicroBooNE. Previous experience from FNAL have shown that a CuBe wire under tension can be reliably bonded to a copper-clad FR4 surface by a combination of solder (electrical connection) and epoxy (mechanical bonding). This bonding technique greatly simplifies the electrical connection to the readout electronics, and it can be easily automated with commercial equipment. Therefore CuBe wire is selected as the wire of choice for the design.

At 150 micrometers diameter, the break tension of a hardened CuBe wire is about 30N. To ensure no wire breakage in the TPC, the nominal operating tension of the wire will be set at 5N. Periodic support structures on the wire frame will limit the unsupported wire length to less than 2m, resulting in less than 0.2mm deflection due to gravitational or electrostatic forces.

Wire Planes

Four planes of wires are installed on each side of an APA as shown in Figure 3.6. A nominal wire pitch of 4.5mm is selected to provide the adequate position resolution while collecting enough charge for a minimum ionizing track to achieve more than the minimum signal-to-noise ratio. The distance between wire planes is also 4.5mm for optimal signal formation. These four planes are labeled (along the direction of electron drift): the grid plane, the first induction plane (U), the second induction plane (V), and the collection plane (X). The wires on the grid and the collection planes are vertically oriented, while the two induction planes are oriented at $\pm 45^o$ to the vertical. This wire layout is shown to be the best for reconstructing beam-neutrino events. The wires on the grid plane are not connected to the readout electronics; they shield the first induction wire plane from being influenced by distant ionizations. The

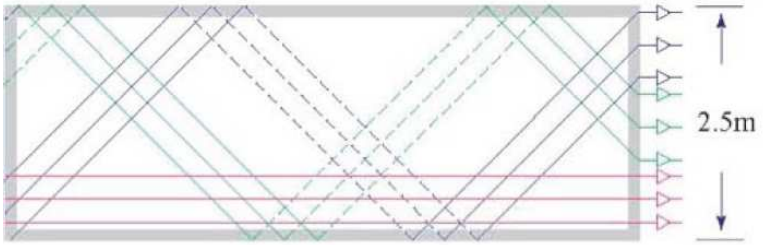

Figure 3.3: Illustration of the wire wrapping around the frame. The APA frame is rotated 90 when installed in the cryostat.

four wire planes will be electrically biased so that electrons from an ionizing-particle track completely drift past the first three planes, and are collected by the fourth plane. The bias voltages needed to achieve this goal are in the range of 0V - 700V. A grounded mesh plane, located 3 mm behind the collection plane, prevents the electric field around this set of wires from being distorted by the metal frame structure and the wires on the opposite side of the frame. The wires on the two induction planes (U & V) are wrapped at $\pm 45^o$ around the long edges of the APA frame (Figure 3.3). This technique makes it possible to place readout electronics only at one narrow edge of a APA frame. It slightly complicates the track reconstruction because the U & V wires are sensitive to tracks on both sides of the APA. The APAs electronics will be located at the top edge of the frame as shown in Figure 3.4.

APA Frames

At a nominal wire tension of 5 N, the the total set of wires exert a force of $\sim 6 \times 10^3$ N/m on the short ends of the APA, and $\sim 2 \times 10^3$ N/m force on the long ends. The wire frame must be able to withstand the wire tension with a minimal distortion and no buckling, while minimizing the thickness of the frame to reduce the resulting dead space. A conceptual design of the wire frame is shown in Figure 3.5. Finite element analysis has shown that the maximum distortion of the frame due to wire tension is under 0.5 mm. The total mass of a frame is about 250 kg. All hollow members of the frame are vented to prevent the creation of a trapped volume.

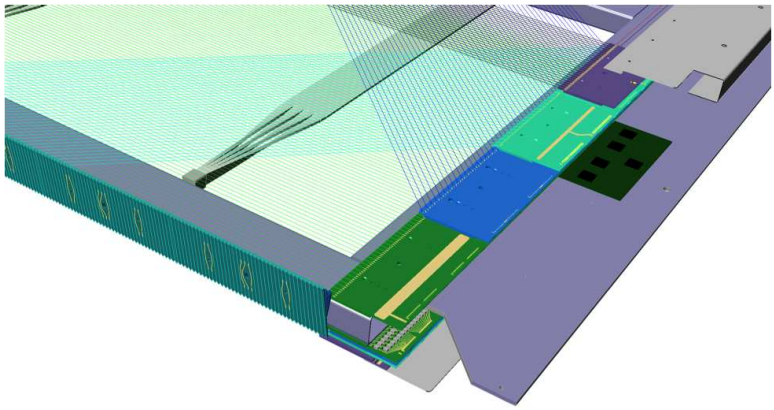

Figure 3.4: Corner view of an APA. Wires strung at 0^o, $+45^o$ and -45^o are attached to circuit boards at the sides and ends of the APA. One of the 10 photon detection system paddles that reside in each APA is shown. One readout board is shown in dark green. A metal cover encloses the readout boards.

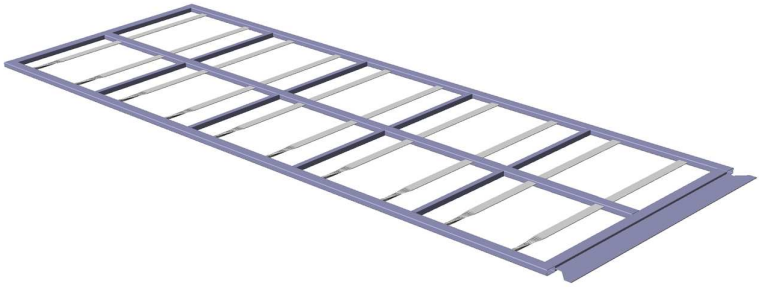

Figure 3.5: Conceptual design of a APA frame with 10 light collection paddles.

Wire Connections at Ends of APA

Figure 3.6 shows three major cross sections of an APA. The top figure is the cross section of the readout end of an APA. The four planes of wires are attached to their respective wire-bonding boards through a combination of solder and epoxy. Copper traces on a wire bonding board connect each of the readout wires to the corresponding pin receptacles on the opposite end of the board. An array of pins on the front-end readout boards is pushed through the stack of wire bonding boards, making electrical connection between the readout electronics and the matching wires. These readout boards process the analog signals from the wires and transmit the digital information through feedthroughs to the DAQ system outside the cryostat. The electronics on the readout boards dissipate an estimated 60W of heat per APA.

The bottom figure shows the cross section of the long end of an APA. Only two layers (U & V) of wire wrapping boards are needed along this edge of the APA. The wire-wrapping boards are made from printed circuit boards. On each of the wire-wrapping board, there are bonding pads for soldering and gluing the wires at the edges. Copper traces interconnect the wires from one side of the APA to those on the other side. This arrangement allows a more convenient placement of mounting holes through the center of the boards. As with the wire-wrapping boards shown in the middle figure, precision curved grooves are machined onto the edge of the boards to guide the wires into the correct position, and to prevent sharp kinks from forming on the wires. Protective guards are placed on the three wrapped edges of an APA during storage and shipment.

Cathode Plane Assemblies (CPAs)

The cathode plane assemblies (CPAs) have the same dimensions as the APAs. Each CPA is made of a stainless-steel framework, with a layer of stainless-steel wire mesh stretched over one side of the frame. To reduce drift field distortions, all surfaces that rise signifcantly above the mesh, including the stainless-steel frame structure on the other side of the mesh, are covered with field-shaping electrodes biased at appropriate voltages. Figure 3.7 illustrates the concept of the cathode plane assembly. A cathode plane voltage of 125kV is required to achieve a drift field of 500 V/cm.

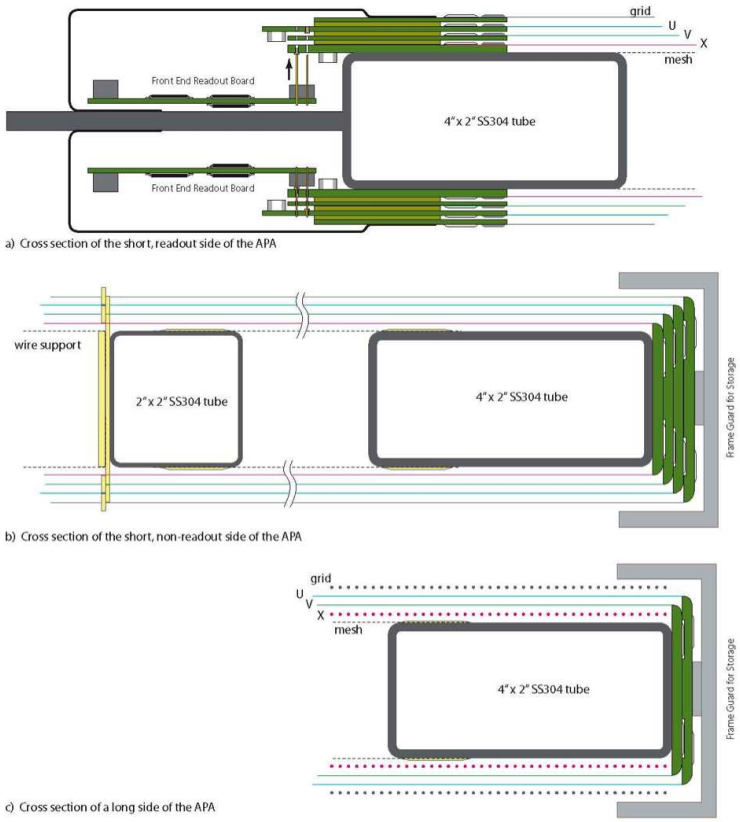

Figure 3.6: Three cross sectional views of the APA showing the attachment of the wire planes.

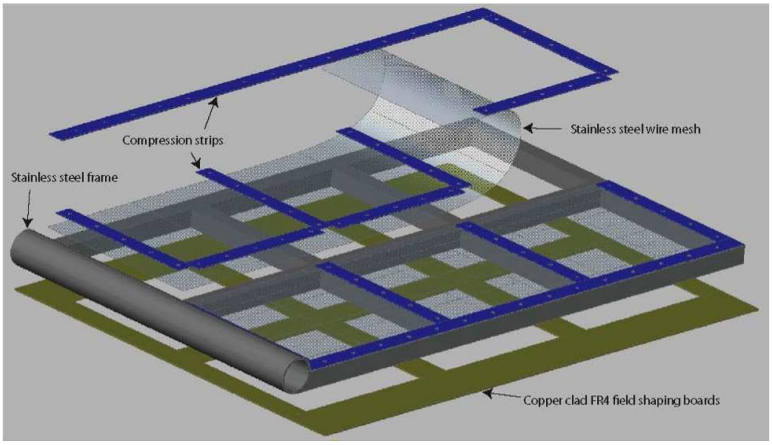

Figure 3.7: Conceptual design of a cathode plane assembly (not to scale)

Field Cages

Each pair of facing cathode and anode rows forms an electron-drift region. A field cage will completely surround the four open sides of this region to provide the necessary boundary conditions to ensure a uniform electric field within, unaffected by the presence of the cryostat walls. We propose to use copper-clad FR4 panels similar to those used in ArgoNeuT and planned for use in LBNE. Parallel copper strips will be etched on the panels and will be biased at appropriate voltages by a resistive divider network. These strips will create a linear electric-potential gradient in the LAr, ensuring a uniform drift field in the TPC active volume. The field cage panels will be mounted on 2.5m long fiberglass I-beams that are assembled with a CPA frame in a hinged fashion as shown in Figure 3.2.

TPC Assembly in the Cryostat

Three mounting rails will be installed in the gas space above the liquid argon and arranged along the beam direction. The central rail supports the two rows of APAs. The outer rails support the three rows of CPAs. The rails are attached to anchor points on the cryostat roof by hanging rods. The mounting rails are separated by 2.5m.

APAs and CPAs are installed by individually 1) lowering them into the cryostat through a hatch located at the top of the cryostat, 2) transferring them to a mounting rail and 3) rolling them into position. The field cage panels are next swung into position and attached to the APAs.

3.3.4 In-Vessel Electronics

The large number of readout channels required to instrument the LAr1 TPC motivates the use of CMOS ASICs for the electronics. These electronics have, to a large extent, already been developed for LBNE and will be used in MicroBooNE. Requirements of low noise (less than 1000 rms electrons for a wire capacitance of 200 pF) and for extreme purity of the LAr dictate that the front-end electronics be located at the signal wires in LAr, which reduces the signal capacitance (thereby minimizing noise).

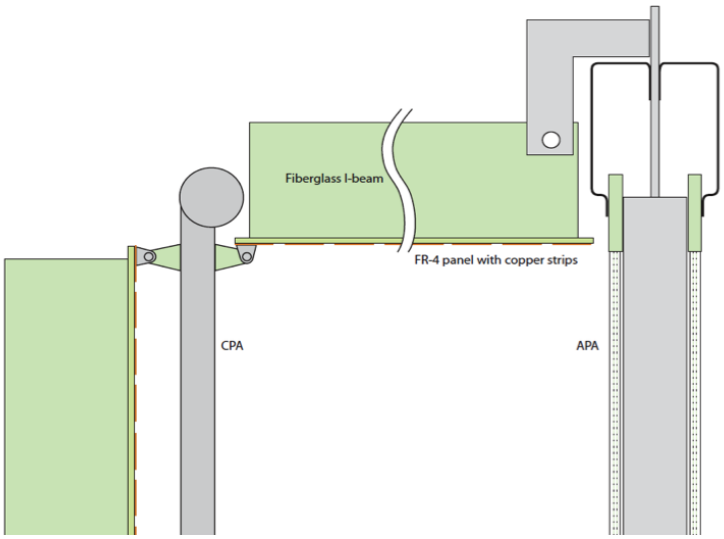

Figure 3.8: Mounting rails to support APAs and CPAs

This electronics architecture, combined with the modular TPC elements, also leads to a TPC implementation that can be readily scaled to any detector size or geometry.

The entire electronics chain is immersed in the LAr and operates at 89 K. It is composed of a 16-channel front-end implemented as a mixed-signal ASIC providing amplification, shaping, digitization, buffering, a 16:1 multiplexing stage, a driver and voltage regulators. Eight front-end ASICs plus a single digital ASIC implementing an 8:1 multiplexer, clock and control circuitry comprise a single 128-channel front-end readout board. A driver/receiver circuit on each motherboard will transmit data out of the cryostat on a twisted copper pair through a feedthrough to the DAQ system, and receive programming instructions from the DAQ system. There will be 20 cable sets for each APA.

Even at the surface, the electronics occupancy in an APA in a full drift time is quite low. An efficient zero-suppression scheme can greatly reduce the total data volume. One scheme can be implemented with a dedicated buffer for each channel having a write-enable consisting of the OR of that channel and its two nearest neighbors. A few samples before and after the write enable would also be recorded to capture the below-threshold leading and trailing edges of the signal waveform. This mode provides maximal zero-suppression that is insensitive to localized low energy events and noise. The in-vessel electronics will be capable of sampling data continuously.

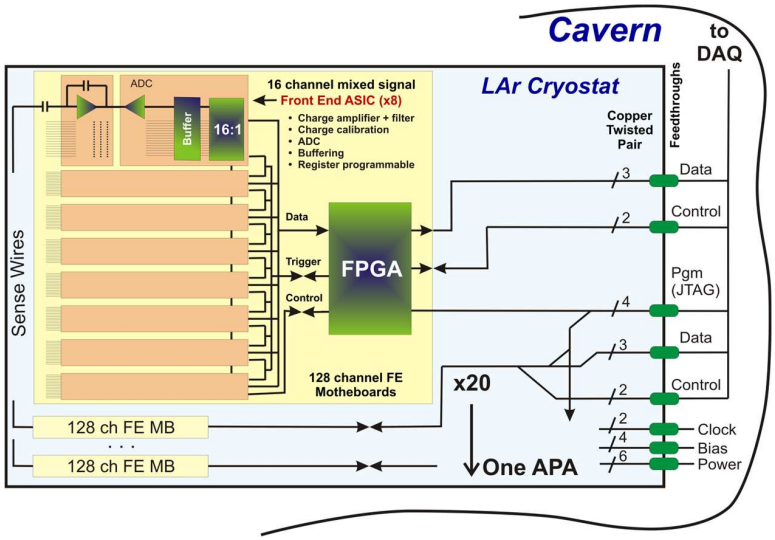

Figure 3.9: Electronics Block Diagram

The data rate will be dominated by cosmic rays (3 - 12 kHz per APA). The rate per front-end mother board is expected to be 50 Mb/s. By comparison, the rate for radioactive decays and electronic noise is expected to be 10 Mb/s per APA. The Ar39 decay rate is 122 kHz/APA. The rate of sampled decays for a 0.5 MIP threshold will be 34kHz.

Figure 3.9 shows a block diagram of the 16-channel front-end ASIC. Each channel includes a charge amplifier with a selectable of gain of 4.7, 7.8, 14 and 25 mV/fC, a high-order anti-aliasing filter with adjustable time constant (peaking time 0.5, 1, 2, and 3 μs), an option to enable an AC coupling, baseline adjustment for operation with either the collecting or the non-collecting wires, a 12-bit 2 MS/s ADC, and a data compression stage. Shared among the 16 channels are the bias circuits, registers, a temperature monitor, the digital multiplexer (16:1), an analog buffer for signal monitoring, and the digital interface. A 600 kb buffer has been assumed in this example, capable of storing a 1.5 ms event sampled at 2 MS/s in each channel assuming no compression. Two or more events can be stored with compression. The power dissipation is less than 15 mW/channel.

A 16-channel ASIC implementing the complete analog front-end section has been designed and fabricated in a commercial CMOS process (0.18 μm and 1.8V). The charge amplification and shaping filter have programmable gain and peaking time.

The ASIC integrates a band-gap reference (BGR), used to generate all the internal bias voltages and currents. This guarantees a high stability of the operating point over a wide range of temperatures, from room temperature to 77 K. The ASIC was packaged in a commercial, fully encapsulated plastic QFP 80 package.

The reference design for the DAQ system is guided by recent experience gained in the development of relevant systems for the NOvA and MicroBooNE experiments, as well as from running experiments with comparable channel counts and/or experimental conditions, such as D-Zero, CDF, MINOS and ICARUS. The DAQ system will be located external to the cryostat vessel, with components in the detector hall and in an on-site control room. It consists of the following components:

- Custom "Data Concentrator Modules "(DCM) located in racks that sit directly above the signal feedthroughs on the roof of the cryostat. The NOvA DCM is suitable for our use with minor modification. These connect to:
- A network consisting of commercial Ethernet switches located in the detector hall and a commercial router located in the counting house/control room, for the transmission of data to:
- A local farm of commodity computers that provide data storage, trigger, event-building and real-time processing/event reconstruction functions,
- A custom timing system consisting of a master unit that locks onto a GPS clock and distributes timing signals to the data concentrator modules via slave units, and
- Dedicated computer nodes that host run control, routing control, node supervisor and slow controls processes.

The reference design of the data acquisition system is summarized in block diagram form in Figure 3.10. The design strives to minimize the impact of single-point failures, and maximize the use of commercial components.

3.3.5 Trigger - Light Collection

Scintillation light is produced copiously in liquid argon at 128 nm. Detection of this light plays several important roles in LArTPCs. For a surface detector in a

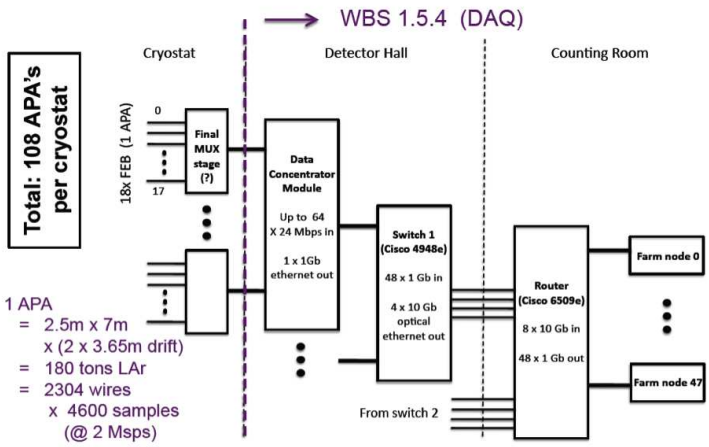

Figure 3.10: DAQ Block Diagram

beam, like LAR1, the scintillation light provides a tag of events in-time with the beam pulse, allowing rejection of cosmic rays. For underground, large LArTPCs, the light provides the T_0 for non-accelerator events (such as supernova events) with no minimum ionizing particle, necessary for reconstructing the event energy.

The traditional method for detecting the scintillation light uses tetraphenyl butadiene (TPB) coatings on photomultiplier tubes (PMTs) or plates placed in front of the PMTs. For example, in the MicroBooNE he coating is applied to a 12-inch diameter acrylic plate positioned directly in front of an 8-inch R5912-mod PMT. This design is known to work well in modest-sized LArTPCs. However in ultra-large detectors, where space is at a premium, a more compact system is desirable.

To address this problem, Ref. [32] describes a lightguide system for detecting scintillation light. Coated acrylic bars are arranged side-by-side as a paddle, and bent to guide light adiabatically to a single 2 inch cryogenic PMT, as shown in Figure 3.11. We use a 7725-mod Hamamatsu, 10-stage phototube with a custom cryogenic base attached at the bottom. This assembly provides a flat-profile light detection system that can be inserted into dead regions between LArTPC wire planes.

The lightguides must be constructed of a TPB-based coating with an index of refraction that was chosen to match acrylic bars. Acrylic was chosen as the substrate because it is resilient to cryogenic cycling and can be easily bent to the required form. Some of the visible light that is emitted when UV photons hit the TPB coating will

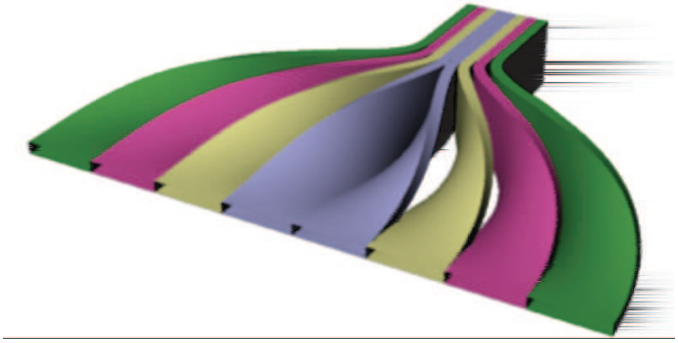

Figure 3.11: Illustration of multiple bars bent to adiabatically guide light to a single PMT.

suffer total internal reflection because the acrylic has an index of refraction for blue light ($n = 1.49$) that is higher than that of liquid argon ($n = 1.23$).

The MIT group has been working on developing improved lightguide coatings from those presented in Ref. [32]. Figure 3.12 shows recent results for observation of prompt scintillation light from a 5 MeV α, where the total acceptance of the light is 7%. To convert from integrated charge to photoelectrons, divide by a factor of 39 and then correct to the appropriate acceptance for light. Our conclusion is that this coating is very promising for sufficient light for triggering/cosmic rejection. The Indiana University group has been developing a system for coating long lightguides, as will be required for LAr1 and industrializing the coating process.

Prototype lightguide paddles are being produced. A muon lifetime measurement will be made with six short (50 cm) paddles at MIT during autumn, 2012. These paddles will then be installed for a long run in MicroBooNE. Longer (2.5 m) paddles will be tested in the 35 kton LAr prototype by Indiana University.

3.3.6 High Voltage

The conceptual design for the HV feedthrough follows the ICARUS and MicroBooNE designs. A standard feedthrough well insulated to below the level of the liquid Argon, and connection to the cathode plane via a cup at the bottom of the feedthrough.

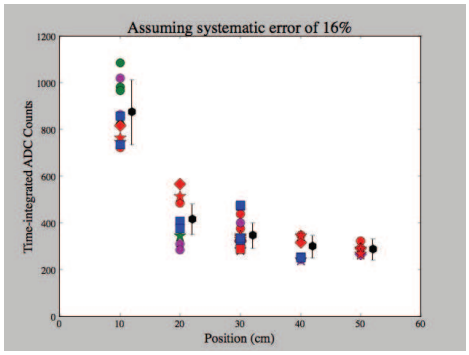

Figure 3.12: Data showing time integrated charge as a function of location of the measurement along a lightguide. Colors indicate various batches of LAr, while symbols indicate different bars with the same coating. Black hexegons indicate the average and error bars indicate a 16% spread which characterizes the variation between the measurements.

3.3.7 UV Laser System

A UV laser system [33] producing laser light tracks to mimic muons will be installed and tested in LAr1. These "ideal muons" can be used for calibration purposes and for deep underground detectors will be very important given the few cosmics available at depth.

3.4 Muon Spectrometer and Cosmic Ray Veto

A muon spectrometer downstream of LAr1 can serve to determine the momentum and sign of outgoing muons from muon-neutrino interactions. This would both help with energy reconstruction for un-contained events, and could measure the wrong-sign component of the beam precisely. There are many possible designs for a muon spectrometer including spectrometers used, for example, in MINOS or OPERA. A cosmic ray veto would also be very useful in tracking cosmic muons through the detector and using these to calibrate the detector. There are many examples of cosmic ray vetoes which would suffice, including, for example, the Double Chooz veto made up of strips of plastic scintillator read out by M64 PMTs.

Chapter 4

Conclusions

This Letter of Intent describes a 1kton fiducial volume LArTPC detector located on the on-axis Booster Neutrino beamline at a baseline of 700m. This detector, LAr1, will also see an off-axis component of the NuMI beam. LAr1 will have both physics goals and engineering goals. The main physics goal of the experiment is to address the MiniBooNE anomalies, primarily the antineutrino anomaly with measurements in conjunction with MicroBooNE, here serving as a near detector for LAr1. The main development goal for LAr1 is as it serves as an engineering prototype for much larger long baseline neutrino LArTPC detectors deployed underground.

The Collaboration hopes to receive encouragement from the Fermilab Director to develop this Letter of Intent into a proposal and to discuss with them the best way to optimize the experiment.

Bibliography

[1] A. Aguilar-Arevalo *et al.* [LSND Collaboration], "Evidence for neutrino oscillations from the observation of anti-neutrino(electron) appearance in a anti-neutrino(muon) beam," Phys. Rev. D **64**, 112007 (2001) [hep-ex/0104049].

[2] A. A. Aguilar-Arevalo *et al.* [MiniBooNE Collaboration], "Unexplained Excess of Electron-Like Events From a 1-GeV Neutrino Beam," Phys. Rev. Lett. **102**, 101802 (2009) [arXiv:0812.2243 [hep-ex]].

[3] A. A. Aguilar-Arevalo *et al.* [MiniBooNE Collaboration], "Event Excess in the MiniBooNE Search for $\bar{\nu}_\mu \to \bar{\nu}_e$ Oscillations," Phys. Rev. Lett. **105**, 181801 (2010) [arXiv:1007.1150 [hep-ex]].

[4] Physical Review C, **83:054615**; Physical Review C, **84:024617** 2011

[5] W. Hampel *et al.* [GALLEX Collaboration], "Final results of the Cr-51 neutrino source experiments in GALLEX," Phys. Lett. B **420**, 114 (1998). , J. N. Abdurashitov *et al.* [SAGE Collaboration], "Measurement of the response of the Russian-American gallium experiment to neutrinos from a Cr-51 source," Phys. Rev. C **59**, 2246 (1999) [hep-ph/9803418].

[6] "Light Sterile Neutrinos: A Whitepaper", arXiv:1204.5379

[7] Future Short-Baseline Neutrino Experiments – Needs and Options: https://indico.fnal.gov/conferenceDisplay.py?confId=5273

[8] Physical Review D, **83:073006**, 2011

[9] See, for example, "Testing the Reactor and Gallium Anomalies: The 4th ν Hypothesis", T. Lasserre, CERN Town Meeting Workshop, May 14th-16th, 2012

[10] C. Giunti and M. Laveder, "3+1 and 3+2 Sterile Neutrino Fits," Phys. Rev. D **84**, 073008 (2011) [arXiv:1107.1452 [hep-ph]].

[11] A. Porta [Nucifer Collaboration], "Reactor neutrino detection for non proliferation with the Nucifer experiment," J. Phys. Conf. Ser. **203** (2010) 012092.

[12] See, for example, "Testing the Reactor and Gallium Anomalies: The 4th ν Hypothesis", T. Lasserre, CERN Town Meeting Workshop, May 14th-16th, 2012

[13] See, for example, "Testing the Reactor and Gallium Anomalies: The 4th ν Hypothesis", T. Lasserre, CERN Town Meeting Workshop, May 14th-16th, 2012

[14] A. Piepke, F. Boehm, M. Chen, B. Cook, H. Henrikson, R. Hertenberger, K. Lou and N. Mascarenhas *et al.*, "The San Onofre reactor neutrino experiment: A low-energy test of the atmospheric neutrino anomaly," In *Osaka 1995, Weak and electromagnetic interactions in nuclei* 599-607

[15] See, for example, "Testing the Reactor and Gallium Anomalies: The 4th ν Hypothesis", T. Lasserre, CERN Town Meeting Workshop, May 14th-16th, 2012

[16] See, for example, "Testing the Reactor and Gallium Anomalies: The 4th ν Hypothesis", T. Lasserre, CERN Town Meeting Workshop, May 14th-16th, 2012

[17] A. P. Serebrov, V. G. Zinoviev, A. K. Fomin, U. E. Loginov, M. S. Onegin, A. M. Gagarsky, G. A. Petrov and V. A. Solovey *et al.*, "NEUTRINO4 experiment: preparations for search for sterile neutrino at 100 MW reactor SM-3 at 6-12 meters," arXiv:1205.2955 [hep-ph].

[18] See, for example, "Testing the Reactor and Gallium Anomalies: The 4th ν Hypothesis", T. Lasserre, CERN Town Meeting Workshop, May 14th-16th, 2012

[19] See, for example, "Testing the Reactor and Gallium Anomalies: The 4th ν Hypothesis", T. Lasserre, CERN Town Meeting Workshop, May 14th-16th, 2012

[20] M. Cribier, M. Fechner, T. Lasserre, A. Letourneau, D. Lhuillier, G. Mention, D. Franco and V. Kornoukhov *et al.*, "A proposed search for a fourth neutrino with a PBq antineutrino source," Phys. Rev. Lett. **107**, 201801 (2011) [arXiv:1107.2335 [hep-ex]].

[21] See, for example, "Testing the Reactor and Gallium Anomalies: The 4th ν Hypothesis", T. Lasserre, CERN Town Meeting Workshop, May 14th-16th, 2012

[22] See, for example, "Testing the Reactor and Gallium Anomalies: The 4th ν Hypothesis", T. Lasserre, CERN Town Meeting Workshop, May 14th-16th, 2012

[23] D. A. Dwyer, K. M. Heeger, B. R. Littlejohn and P. Vogel, "Search for Sterile Neutrinos with a Radioactive Source at Daya Bay," arXiv:1109.6036 [hep-ex].

[24] H. Ray [OscSNS Collaboration], "OscSNS: Precision Neutrino Measurements at the Spallation Neutron Source," J. Phys. Conf. Ser. **136**, 022029 (2008) [arXiv:0810.3175 [hep-ex]].

[25] A. Bungau, A. Adelmann, J. R. Alonso, W. Barletta, R. Barlow, L. Bartoszek, L. Calabretta and A. Calanna *et al.*, "An Electron Antineutrino Disappearance Search Using High-Rate 8Li Production and Decay," arXiv:1205.4419 [hep-ex].

[26] H. Chen *et al.* [MicroBooNE Collaboration], "Proposal for a New Experiment Using the Booster and NuMI Neutrino Beamlines: MicroBooNE," FERMILAB-PROPOSAL-0974.

[27] G. Tzanankos *et al.* [MINOS+ Collaboration], "MINOS+: a Proposal to FNAL to run MINOS with the medium energy NuMI beam," FERMILAB-PROPOSAL-1016.

[28] M. Antonello, D. Bagliani, B. Baibussinov, H. Bilokon, F. Boffelli, M. Bonesini, E. Calligarich and N. Canci *et al.*, "Search for 'anomalies' from neutrino and anti-neutrino oscillations at Delta_m^2 1eV^2 with muon spectrometers and large LAr-TPC imaging detectors," arXiv:1203.3432 [physics.ins-det].

[29] Fermilab Long Baseline Neutrino Experiment, http://lbne.fnal.gov/.

[30] B. Rebel, M. Adamowski, W. Jaskierny, H. Jostlein, C. Kendziora, R. Plunkett, S. Pordes and R. Schmitt *et al.*, "Results from the Fermilab materials test stand and status of the liquid argon purity demonstrator," J. Phys. Conf. Ser. **308**, 012023 (2011).

[31] F. Arneodo [ICARUS Collaboration], "The ICARUS T600 liquid Argon time projection chamber," Nucl. Instrum. Meth. A **525**, 118 (2004).

[32] "Demonstration of a Lightguide Detector for Liquid Argon TPCs," L. Bugel, J.M. Conrad, C. Ignarra, B.J.P. Jones, T. Katori, T. Smidt, H.-K. Tanaka, arXiv:1101.3013 [physics.ins-det] , Nucl. Inst. Meth., 640:1, 69, 2011.

[33] B. Rossi, I. Badhress, A. Ereditato, S. Haug, R. Hanni, M. Hess, S. Janos and F. Juget *et al.*, "A Prototype liquid Argon Time Projection Chamber for the study of UV laser multi-photonic ionization," JINST **4**, P07011 (2009) [arXiv:0906.3437 [physics.ins-det]].